Orbital hybridized topological Fulde-Ferrel superfluidity in a noncentrosymmetric optical lattice

Bo Liu,[1,2] Xiaopeng Li,[3] and W. Vincent Liu[1,2]

[1]*Department of Physics and Astronomy, University of Pittsburgh, Pittsburgh, PA 15260, USA*
[2]*Wilczek Quantum Center, Zhejiang University of Technology, Hangzhou 310023, China*
[3]*Condensed Matter Theory Center and Joint Quantum Institute, University of Maryland, College Park, MD 20742, USA*

(Dated: May 28, 2015)

Topological phases like topological insulators or superconductors are fascinating quantum states of matter, featuring novel properties such as emergent chiral edge states or Majorana fermions with non-Abelian braiding statistics. The recent experimental implementation of optical lattices with highly tunable geometry in cold gases opens up a new thrust on exploring these novel quantum states. Here we report that the topological non-trivial Bloch bands can arise naturally in a noncentrosymmetric lattice. It induces a controllable orbital hybridization, producing the topological band structure. In such bands, when considering attractive fermionic atoms, we find a topological Fulde-Ferrell superfluid state with finite center-of-mass momentum in the presence of onsite rotation. This topological superfluid supports Majorana fermions on its edges. Experimental signatures are predicted for cold gases in radio-frequency spectroscopy.

Symmetry plays an important role in solid state materials and influences many of their properties in a profound way. Recently, the noncentrosymmetric materials, i.e., crystal structure lacking a center of inversion, have attracted considerable theoretical and experimental attention in various fields of condensed matter physics [1]. In contrast to the centrosymmetric case, the absence of inversion symmetry leads to very rich physical phenomena, such as skyrmion states [2–4], novel superconducting phases [5–8], as well as magnetoelectric effect [9, 10]. In parallel to the developments in solid state physics, optical lattices with highly tunable geometry in the recent ultracold atom experiments [11] provide new opportunities to study noncentrosymmetric materials. Taking the advantage of high controllability, the cold gases are expected to emerge not only as a flexible tool to simulate electronic system, but also a versatile platform to create fascinating quantum states of matter not existing in nature.

Recent experimental progress in manipulating higher orbital bands in optical lattices [12–16] provides unprecedented opportunities to investigate quantum many-body phases with orbital degrees of freedom. Studying higher orbital physics in optical lattices is attracting considerable interests due to their unique and intrinsic spatial nature [17]. An idea of using orbital hybridization to emulate spin-orbit physics, or artificial gauge fields in general, has emerged in recent theoretical studies [18–22], where various interesting many-body states have been proposed. In the context of periodically driven systems, orbital hybridization is shown to be controllable by lattice shaking [23–25]. However how to systematically control the orbital hybridization in static optical lattices remains unclear and stands as an obstacle to explore the rich phenomena in orbital hybridized many-body ground states.

In this letter, we propose a static noncentrosymmetric optical lattice, where the orbital hybridization is systematically controllable by manipulating symmetry breaking. We find topological bands arise from the interplay between high orbitals and inversion symmetry breaking, yet without requiring Raman induced spin-orbit coupling nor other artificial gauge field [26, 27]. Furthermore when considering attractive fermionic atoms, say ^{6}Li [28–31] loaded into such a noncentrosymmetric optical lattice, we find an orbital hybridized topological Fulde-Ferrell superfluid state (tFF) in the presence of local orbital angular momentum induced by onsite rotation [32]. This state represents an unconventional type of Fulde-Ferrell-Larkin-Ovchinnikov (FFLO) state, topologically distinct from the s-wave FFLO superfluidity observed in a quasi-one dimensional Fermi gas [29]. This orbital realization of the tFF superfluid state here is distinguished from previous works based on hyperfine states [33–35], where spin-orbit coupling and Zeeman fields are required. Moreover, our symmetry-based method of controlling orbital hybridization is in principle applicable to other optical lattice setups as well [18–22, 36, 37], which could lead to more interesting noncentrosymmetric many-body phases worth future exploring.

Effective model. Let us consider a noncentrosymmetric optical lattice with the potential

$$\begin{aligned} V(x,y) &= -V_X \cos^2(k_{Lx}x) - V_Y \cos^2(k_{Ly}y) \\ &+ V_{\bar{Y}} \cos^2(3k_{Ly}y + \theta/2), \end{aligned} \tag{1}$$

where V_X, V_Y, $V_{\bar{Y}}$ are the depth of optical lattices, k_{Lx}, k_{Ly} are the wavevectors of laser fields and the corresponding lattice constants are $a_x = \pi/k_{Lx}$, $a_y = \pi/k_{Ly}$ along x and y directions respectively. By the techniques of designing the geometry of optical lattices developed in the recent experimental advances [11], the configuration of optical lattices considered here can be formed through three retro-reflected laser beams as shown in Fig. 1(a). The interference of two perpendicular beams X and Y gives rise to a 2D square lattice. The third beam $\bar{Y}$ creates an additional standing wave pattern which breaks the inversion symmetry along the y direction, for example, when $\theta = \pi/2$ as shown in Fig. 1(b). This noncentrosymmetric geometry plays a crucial role in producing the non-trivial Bloch bands in our model, to be illustrated below. Here we consider highly anisotropic geometry of the optical lattice through increasing lattice depth ($V_Y \gg V_X$) and spacing ($a_y \gg a_x$) in the y direction, meanwhile requiring that the lattice potential satisfy the condition $V_X k_{Lx}^2 = V_Y k_{Ly}^2$. This should keep local rotational symmetry of each site in the

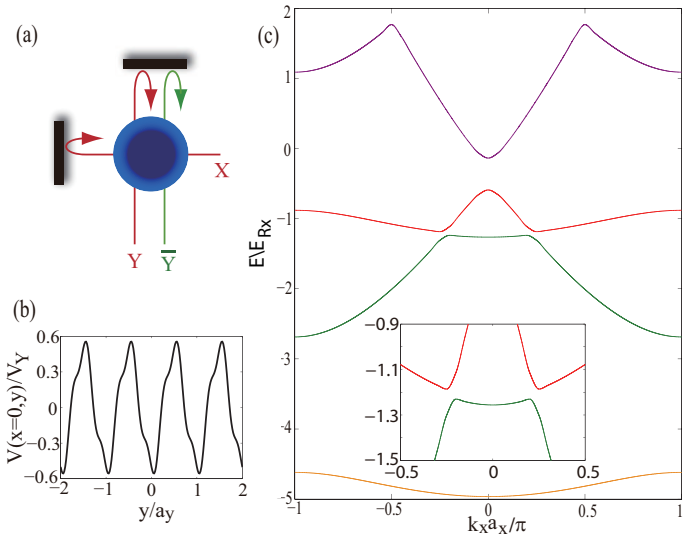

FIG. 1: Noncentrosymmetric optical lattice and topological band structures. (a) Three retro-reflected laser beams create the lattice potential in Eq. (1). X and Y interfere and produce a 2D square lattice, while $\bar{Y}$ creates an independent standing wave. (b) Lattice potential along the y direction shows the inversion symmetry breaking. (c) The single-particle energy spectrum along k_x axis in the unit of E_{Rx} for the lowest four bands through plane wave expansion calculation. Here the lattice depth is chosen as $V_X/E_{Rx} = 4$, $V_Y/E_{Ry} = 40$ and $V_{\bar{Y}}/E_{Ry} = 4$ with the recoil energy $E_{Rx} = \hbar^2 k_{Lx}^2/2m$ and $E_{Ry} = \hbar^2 k_{Ly}^2/2m$.

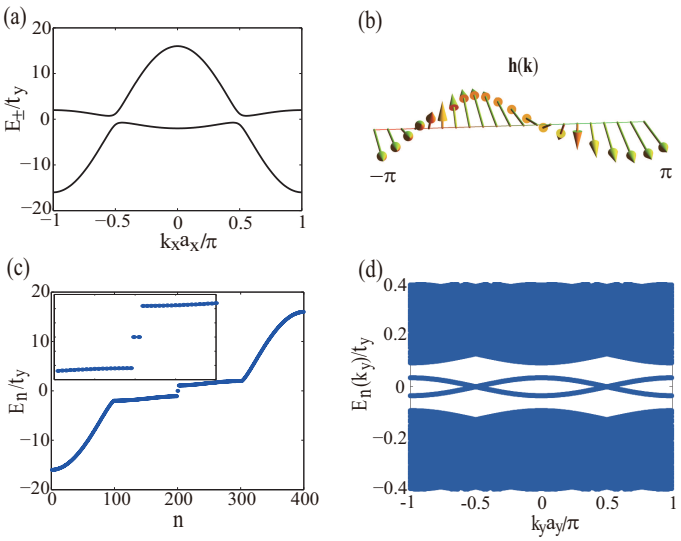

FIG. 2: Bulk and edge properties of the topological band insulator. (a) The single-particle band structure calculated from the tight binding model (Eq. (2)) in quasi-1D limit, when $t_x/t_y = 8$, $t/t_y = 0.6$. (b) Topological winding of Hamiltonian in Eq. (3) across the Brillouin zone. (c) Energy spectrum of the Hamiltonian (Eq. (2)) in quasi-1D limit with finite length (lattice sites $N = 200$), when $t_x/t_y = 8$ and $t/t_y = 0.9$. There are two zero-energy states inside the gap which are located at the two outer edges of the system respectively. Here n labels the energy level. (d) The effect of the small transverse tunneling. The midgap bands show a finite curvature along the y direction with open (and periodic) boundary conditions in the x (y) directions when $t_x/t_y = 8$, $t/t_y = 0.1$, $t'_y/t_y = 0.02$ and $t'_x/t'_y = 0.1$.

xy plane [36]. The band structure of such a lattice system is solved numerically through plane wave expansion. We find that the second and third bands cross in the absence of $V_{\bar{Y}}$ with the band touching points protected by time-reversal and inversion symmetries. With finite $V_{\bar{Y}}$, we see the gap reopening due to inversion symmetry breaking (Fig. 1(c)). The band mixing can thus be turned on and off by controlling the symmetry of the lattice geometry.

The essential physics of band mixing is captured by the following multi-orbital tight binding model without considering the full band structure theory,

$$\begin{aligned} H_0 &= t_x \sum_{\mathbf{r}} C^\dagger_{p_x}(\mathbf{r}) C_{p_x}(\mathbf{r}+\vec{e}_x) - t_y \sum_{\mathbf{r}} C^\dagger_{p_y}(\mathbf{r}) C_{p_y}(\mathbf{r}+\vec{e}_x) \\ &+ t \sum_{\mathbf{r}} C^\dagger_{p_x}(\mathbf{r}) C_{p_y}(\mathbf{r}+\vec{e}_x) - t \sum_{\mathbf{r}} C^\dagger_{p_y}(\mathbf{r}) C_{p_x}(\mathbf{r}+\vec{e}_x) \\ &- t'_x \sum_{\mathbf{r}} C^\dagger_{p_x}(\mathbf{r}) C_{p_x}(\mathbf{r}+\vec{e}_y) + t'_y \sum_{\mathbf{r}} C^\dagger_{p_y}(\mathbf{r}) C_{p_y}(\mathbf{r}+\vec{e}_y) \\ &+ h.c. - \mu \sum_{\mathbf{r}} [C^\dagger_{p_x}(\mathbf{r}) C_{p_x}(\mathbf{r}) + C^\dagger_{p_y}(\mathbf{r}) C_{p_y}(\mathbf{r})], \end{aligned} \tag{2}$$

where $C_\nu(\mathbf{r})$ is a fermionic annihilation operator for the localized ν orbital (p_x or p_y) located at the lattice site $\mathbf{r}$ and the chemical potential is denoted by μ. Since the system is relatively stronger confined in the y direction, the tunnelings (t'_x, t'_y) in the y direction are much weaker compared to that (t_x, t_y) along the x direction. The relative sign of the hopping amplitude is fixed by the parity of p_x and p_y orbitals. The key ingredient in our model is the hybridization between p_x and p_y orbitals. It arises from the asymmetric shape of the p_y orbital wavefunction induced by the inversion symmetry breaking in the y direction. This asymmetry leads to the orbital hybridization $t\sum_{\mathbf{r}}[C^\dagger_{p_x}(\mathbf{r})C_{p_y}(\mathbf{r}+\vec{e}_x) - C^\dagger_{p_y}(\mathbf{r})C_{p_x}(\mathbf{r}+\vec{e}_x)] + h.c.$ in Eq. (2), which plays a crucial role in producing topological non-trivial band structures. It resembles spin-orbit coupling [38–40] when the p_x and p_y orbitals are mapped to pseudo-spin-1/2 states. But unlike the spin-orbit coupling, the orbital hybridization is geometrically controllable through manipulating the inversion symmetry of the optical lattice.

Topological band structures. We first focus on the quasi-one dimensional limit where the transverse (y direction) tunnelings are negligible. At half filling (one particle per lattice site), in the basis of $(C^\dagger_{p_x}(\mathbf{k}), C^\dagger_{p_y}(\mathbf{k}))$, the Hamiltonian takes a suggestive form

$$H_0(\mathbf{k}) = h_0(\mathbf{k})\mathbb{I} + \mathbf{h}(\mathbf{k}) \cdot \sigma, \tag{3}$$

where $h_0(\mathbf{k}) = (t_x - t_y)\cos(k_x a_x)$, $h_x(\mathbf{k}) = 0$, $h_y(\mathbf{k}) = -2t\sin(k_x a_x)$, $h_z(\mathbf{k}) = (t_x + t_y)\cos(k_x a_x)$, and $\sigma_{x,y,z}$ are Pauli matrices. The energy spectrum reads $E_\pm = h_0(\mathbf{k}) \pm \sqrt{h_y^2(\mathbf{k}) + h_z^2(\mathbf{k})}$. As shown in Fig. 2(a), the system is in an insulating state with a band gap determined by the orbital hy-

bridization t. It is a Z_2 topological insulator protected by time reversal and reflection symmetries [41]. To visualize the topological properties of the band structures, we show the vector $\mathbf{h}(\mathbf{k})$ winds an angle of 2π when the momentum $\mathbf{k}$ varies from $-\pi$ to π crossing the entire Brillouin zone (BZ) in Fig. 2(b). It is also confirmed from the calculation of winding number defined as $W = \oint \frac{dk_x}{4\pi} \epsilon_{\eta\eta'} \hat{h}_\eta^{-1}(k_x) \partial_{k_x} \hat{h}_\eta$ with $\hat{h} \equiv \frac{\mathbf{h}}{|\mathbf{h}|}$ and $\epsilon_{yz} = -\epsilon_{zy} = 1$. When $t \neq 0$, the winding number is 1, which signifies a topological band insulator state. The nontrivial topology of this state also manifests through the existence of the edge states. As shown in Fig. 2(c), there are two emergent zero-energy modes located at the two outer edges of the system respectively.

Next we will discuss the effect of the small transverse (y direction) tunneling, which has been neglected above but always exists in a realistic quasi-one dimensional system. By considering small transverse tunneling, the zero-energy modes of individual chain will morph into a midgap band, with finite curvature in the transverse direction as shown in Fig. 2(d). The topological band insulator state remains stable at small value of transverse tunneling. For example, when $t_x/t_y = 8$ and $t/t_y = 0.1$, the topological state survives until t'_y/t_y reaches 0.073 with $t'_x = 0.1t'_y$. However, beyond this value, the band gap will close and the topological band insulator state becomes unstable.

Topological Fulde-Ferrell state and Majorana fermions. In this section, we study attractive fermions in the topological noncentrosymmetric optical lattice (Eq. (1)) with onsite rotation [32] and show that a topological Fulde-Ferrell superfluid state (tFF) with finite center-of-mass momentum emerges. The interacting model to describe this fermionic system is

$$H = H_0 + H_{int} + H_L + H_Z. \tag{4}$$

In this model, the interaction $H_{int} = U \sum_{\mathbf{r}} C^\dagger_{p_x}(\mathbf{r}) C_{p_x}(\mathbf{r}) C^\dagger_{p_y}(\mathbf{r}) C_{p_y}(\mathbf{r})$ can be induced by considering optical Feshbach resonance [42, 43], Bose-Fermi mixtures [44] or dipolar atoms\molecules [45]. $H_L = i\Omega_z \sum_{\mathbf{r}} [C^\dagger_{p_x}(\mathbf{r}) C_{p_y}(\mathbf{r}) - C^\dagger_{p_y}(\mathbf{r}) C_{p_x}(\mathbf{r})]$ is the onsite rotation induced orbital Zeeman energy. H_Z is the orbital splitting $h \sum_{\mathbf{r}} [C^\dagger_{p_x}(\mathbf{r}) C_{p_x}(\mathbf{r}) - C^\dagger_{p_y}(\mathbf{r}) C_{p_y}(\mathbf{r})]$ originated from the onsite energy difference between p_x and p_y orbitals, which is tunable through adjusting the lattice depth or lattice spacing in x and y directions. In the presence of onsite rotation, i.e., $\Omega_z \neq 0$, the Fermi surface of the system becomes asymmetric along the x direction. The pairing with the center-of-mass momentum $\mathbf{Q}$ and $-\mathbf{Q}$ are no longer degenerate. The Fulde-Ferrell (FF) state with a plane wave order parameter $\propto e^{i\mathbf{Q}\cdot\mathbf{r}}$ is more energetically favorable as compared to the Larkin-Ovchinnikov state with a stripe order $\propto \cos(\mathbf{Q}\cdot\mathbf{r})$.

Taking the superfluid pairing order parameter $\Delta(\mathbf{r}) = U\langle C_{p_y}(\mathbf{r}) C_{p_x}(\mathbf{r})\rangle = \Delta e^{i\mathbf{Q}\cdot\mathbf{r}}$, the system is described by the Bogoliubov-de-Genes (BdG) Hamiltonian at mean field level. Since the weak transverse hopping introduces a small Fermi surface curvature, we expect the center-of-mass momentum of pairing $\mathbf{Q}$ pointing along the x direction, say $\mathbf{Q} = Q(1, 0)$, in order to maximize the phase space of pairing. Through diagonalizing the BdG Hamiltonian, we obtain the free energy of the system. The pairing order parameter Δ and the center-of-mass momentum of pairing $\mathbf{Q}$ are determined from minimizing the free energy. The details are given in the Supplemental Material. We find that when $\Omega_z > 0$ the center-of-mass momentum of pairing along the x direction is selected as a certain positive Q due to the deformation of the Fermi surface. Since the p_x and p_y bands have different bandwidths, we introduce two dimensionless quantities $\tilde{\mu}_{p_x} = \frac{\mu - h}{2t_x}$ and $\tilde{\mu}_{p_y} = \frac{\mu + h}{2t_y}$, which respectively control the average filling of the two p bands. Correspondingly, we also introduce a dimensionless chemical potential $\tilde{\mu} = \frac{\tilde{\mu}_{p_x} + \tilde{\mu}_{p_y}}{2}$ and orbital polarization $\tilde{h} = \frac{\tilde{\mu}_{p_y} - \tilde{\mu}_{p_x}}{2}$. For fixed $\tilde{\mu}$, the resulting phase diagram as a function of $\tilde{h}$ and the orbital hybridization t is shown in Fig. 3(a). There are two first order phase transitions as the polarization $\tilde{h}$ is increased (except at $t/t_y \approx 0.8$). The first one is a transition from a gapped FF superfluid to a gapless FF superfluid state (with Bogoliubov quasi-particles being gapless). The gap closing across the phase transition is shown in Fig. 3(b). Further increasing the polarization, the second one occurs between the gapless FF and tFF superfluid states. When $t/t_y \approx 0.8$, there is only one phase transition from FF to tFF superfluid states without passing through the gapless FF superfluids, since we find in Fig. 3(c) that E_g will firstly close and reopen immediately. We also find that a finite polarization is required to stabilize the tFF superfluid state. The critical polarization $\tilde{h}_c$ decreases as the orbital hybridization t increases.

The transition from non-topological to topological FF states here can be understood by observing the non-trivial Z_2 topological invariant. The BdG Hamiltonian (See details in the Supplemental Material) maintains the particle-hole symmetry, i.e., $\Xi H_{BdG}(\mathbf{k})\Xi^{-1} = -H^*_{BdG}(-\mathbf{k})$, with $\Xi = \begin{pmatrix} 0 & \mathbb{I} \\ \mathbb{I} & 0 \end{pmatrix}$, while the time reversal and chiral symmetries are broken. Therefore, the tFF superfluid state predicated here belongs to the D symmetry class according to the general classification scheme of topological superconductors [41]. This topological state is thus characterized by a Z_2 topological invariant [46, 47]. As shown in Fig. 3(b) and (c), we find that the Z_2 topological invariant $M = -1$ in the tFF superfluid state (see details in the Supplemental Material).

To further demonstrate the topological nature of the tFF superfluid phase, we will show Majorana fermions are supported in this state. To see this, we consider a cylinder geometry of the system, where the open (periodic) boundary condition is chosen in the $x(y)$ direction respectively. The energy spectrum in Fig. 4(a) is labeled by the momentum k_y. As shown in Fig. 4(a), all the bulk modes are gapped and there are two degenerate flat bands composed of Majorana fermions located at the two outer edges of the system respectively. As shown in Fig. 4(c), for a fixed k_y, there are two zero-energy states located at the two outer edges of the system. The corresponding wavefunctions $(u_{0,\nu}, v_{0,\nu})^T$ satisfy the relation $u_{0,\nu}(x) = v^*_{0,\nu}(x)$ [$u_{0,\nu}(x) = -v^*_{0,\nu}(x)$] on the right [left] edge (Fig. 4(d) and (e)). These eigenstates support localized Majorana fermions at the edges of the system. These

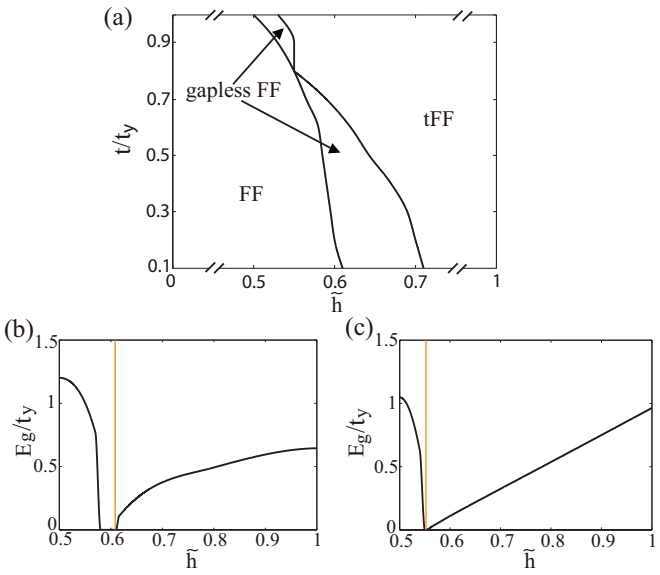

FIG. 3: Zero-temperature phase diagram with fixed $\tilde{\mu}$. (a) When the polarization $\tilde{h}$ is small, the FF superfluid state is the ground state of the system. By increasing $\tilde{h}$, a first order phase transition occurs between FF superfluidity and a gapless FF superfluid state. Further increasing $\tilde{h}$, the system eventually evolves into topological FF superfluid state (tFF). Other parameters are $t_x/t_y = 8$, $t'_y/t_y = 0.05$, $t'_x/t'_y = 0.1$, $U/t_y = -15$, $\tilde{\mu} = 0.4$, and $\Omega_z/t_y = 0.3$. (b) and (c) The quasi-particle exaction gap E_g as a function of polarization $\tilde{h}$ when $t/t_y = 0.6$ and $t/t_y = 0.8$ respectively. The vertical lines mark the point where the Z_2 topological invariant changes.

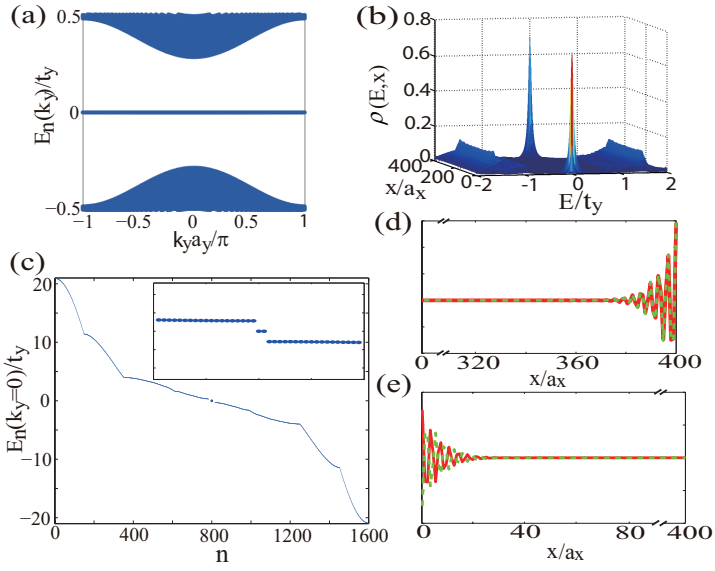

FIG. 4: Topologically protected edge states composed of Majorana fermions in the tFF superfluid state. (a) Energy spectrum of the Hamiltonian in Eq. (4) under the mean-field approximation with open (and periodic) boundary conditions in the x (y) directions. There is a doubly degenerate flat band composed of Majorana fermions when the transverse tunneling is small. (b) The local density of states (LDOS) (see the main text). The zero-energy peaks of the LDOS are located at the two edges of the system respectively. (c) Energy spectra with $k_y a_y = 0$. There are two degenerate zero energy states. (d) and (e), The wavefunctions of the two Majorana zero-energy modes as shown in (c), which satisfy $u_{0,p_x} = v^*_{0,p_x}$ at the right edge and $u_{0,p_x} = -v^*_{0,p_x}$ at the left edge (other components of these two wavefunctions, say u_{0,p_y} and v_{0,p_y}, also satisfy the same relations). These two states support two local Majorana fermions at two outer edges of the system respectively. Here we choose finite length along the x direction with lattice sites $N = 400$ and $\tilde{h} = 0.7$, $t/t_y = 0.6$. Other parameters are the same as in Fig. 3 and n denotes the energy level.

Majorana fermions are signified through the local density of states (LDOS) which can be measured by radio-frequency (rf) spectroscopy [48–50]. The LDOS is calculated as $\rho(x, E) = 1/2 \sum_{n,\nu} \int dk_y [|u_{n,\nu}|^2 \delta(E - \zeta_n) + |v_{n,\nu}|^2 \delta(E + \zeta_n)]$, where $(u_{n,\nu}, v_{n,\nu})^T$ is the eigenvector corresponding to the eigenenergy ζ_n of the mean-field BdG Hamiltonian with cylinder geometry. We find that the zero-energy Majorana fermions manifest themselves by a peak in LDOS located at the edges of the system, as shown in Fig. 4(b). This spatially localized zero-energy peak in LDOS can be detected using spatially resolved radio-frequency (rf) spectroscopy technique [50], which would provide a concrete signature for the experiment.

We also consider the effect of small transverse tunneling on the stability of tFF superfluids. The transverse hopping term restores the 2D nature of the Fermi surface, which acquires a finite curvature in the transverse direction. It suppresses the perfect nesting, therefore it disfavors the tFF superfluid state. Our numerical result indicates that the tFF superfluity remains stable at small value of transverse tunneling. For example, the tFF superfluid state, as shown in Fig. 3(a) with $t/t_y = 0.8$ and $\tilde{h} = 0.7$, survives until t'_y/t_y reaches 0.2 and the flat bands composed of Majorana fermions in a cylinder geometry will be maintained [51]. Beyond this value, the bulk gap will close and the tFF superfluids become unstable.

We would like to emphasize that the topological non-trivial properties in the noncentrosymmetric optical lattice arise directly from symmetry-breaking induced orbital hybridization. This plays a curial role in producing the topological FF superfluid state. We expect noncentrosymmetric optical lattices would provide a fertile ground to support orbital hybridized topological phases in general.

Conclusion. We have established a systematic approach to control non-trivial orbital hybridization in a static noncentrosymmetric optical lattice, which is shown to give rise to unconventional topological properties. We find that this lattice system in the presence of onsite rotation supports a novel topological FF superfluid state when loaded with attractive fermions. It features Majorana zero energy modes located at the outer edges, leading to signatures in the local density of states as a concrete experimental evidence of the topological superfluid state.

Acknowledgement. This work is supported by AFOSR (FA9550-12-1-0079), ARO (W911NF-11-1-0230), Overseas Collaboration Program of NSF of China No. 11429402 sponsored by Peking University, the Charles E. Kaufman Foun-

dation, and The Pittsburgh Foundation (B. L. and W. V. L.). X. L. is supported by LPS-MPO-CMTC, JQI-NSF-PFC and ARO- Atomtronics-MURI.

Supplementary Materials

S-1. BDG EQUATION IN MOMENTUM SPACE

Through introducing the superfluid pairing order parameter $\Delta(\mathbf{r}) = U\langle C_{p_y}(\mathbf{r})C_{p_x}(\mathbf{r})\rangle = \Delta e^{i\mathbf{Q}\cdot\mathbf{r}}$, the system can be described by the Bogoliubov-de-Genes (BdG) Hamiltonian at mean field level

$$H_{BdG}(\mathbf{k}) = \frac{1}{2}\begin{pmatrix} \varepsilon_{p_x}(\mathbf{Q/2}+\mathbf{k}) & \varepsilon(\mathbf{Q/2}+\mathbf{k}) & 0 & \Delta \\ -\varepsilon(\mathbf{Q/2}+\mathbf{k}) & \varepsilon_{p_y}(\mathbf{Q/2}+\mathbf{k}) & -\Delta & 0 \\ 0 & -\Delta^* & -\varepsilon_{p_x}(\mathbf{Q/2}-\mathbf{k}) & \varepsilon(\mathbf{Q/2}-\mathbf{k}) \\ \Delta^* & 0 & -\varepsilon(\mathbf{Q/2}-\mathbf{k}) & -\varepsilon_{p_y}(\mathbf{Q/2}-\mathbf{k}) \end{pmatrix}, \tag{S1}$$

where the Nambu basis is chosen to be $(C_{p_x}(\mathbf{Q/2}+\mathbf{k}), C_{p_y}(\mathbf{Q/2}+\mathbf{k}),\ C^\dagger_{p_x}(\mathbf{Q/2}-\mathbf{k}), C^\dagger_{p_y}(\mathbf{Q/2}-\mathbf{k}))^T$, $\varepsilon_{p_x}(\mathbf{k}) = 2t_x\cos(k_xa_x) - 2t'_x\cos(k_ya_y) - (\mu - h)$, $\varepsilon_{p_y}(\mathbf{k}) = -2t_y\cos(k_xa_x) + 2t'_y\cos(k_ya_y) - (\mu + h)$ and $\varepsilon(\mathbf{k}) = 2it\sin(k_xa_x) + i\Omega_z$.

Then, the free energy can be obtained by diagonalizing the BdG Hamiltonian in Eq. (S1) by standard procedure as

$$F[\Delta] \ = \ 1/2\sum_{\mathbf{k}}[\varepsilon_{p_x}(\mathbf{k}) + \varepsilon_{p_y}(\mathbf{k}) + \sum_{\lambda}\Theta(-E_\lambda(\mathbf{k}))E_\lambda(\mathbf{k})] - \frac{N|\Delta|^2}{U},$$

where E_λ is the quasi-particle energy, and Θ is the Heaviside step function. The pairing order parameter Δ and the center-of-mass momentum of pairing $\mathbf{Q}$ can be determined from minimizing the free energy.

S-2. Z_2 TOPOLOGICAL INVARIANT

To characterize the topological nature of the tFF superfluid state, we calculate the Z_2 topological invariant. Here, we introduce the Majorana operators as $\gamma^A(\mathbf{r}) = C^\dagger_{p_x}(\mathbf{r}) + C_{p_x}(\mathbf{r})$, $\gamma^B(\mathbf{r}) = [C_{p_x}(\mathbf{r}) - C^\dagger_{p_x}(\mathbf{r})]/i$, $\gamma^C(\mathbf{r}) = C^\dagger_{p_y}(\mathbf{r}) + C_{p_y}(\mathbf{r})$ and $\gamma^D(\mathbf{r}) = [C_{p_y}(\mathbf{r}) - C^\dagger_{p_y}(\mathbf{r})]/i$, which fulfill the relations $\gamma^{\dagger\alpha}(\mathbf{r}) = \gamma^\alpha(\mathbf{r})$ and the anticommutation relations $\{\gamma^\alpha, \gamma^\beta\} = 2\delta_{\alpha\beta}\delta(\mathbf{r}-\mathbf{r}')$ with α or β taking A, B, C or D. In terms of Majorana operators, the Hamiltonian in Eq. (4) under the mean-flied approximation can be represented as $H_{MF} = \frac{i}{4}\sum_{l,m=1}^{4N} A_{lm}\gamma_l\gamma_m$ with $\gamma_{4j-3} = \gamma^A(\mathbf{r}_j)$, $\gamma_{4j-2} = \gamma^B(\mathbf{r}_j)$, $\gamma_{4j-1} = \gamma^C(\mathbf{r}_j)$ and $\gamma_{4j} = \gamma^D(\mathbf{r}_j)$, where j runs over all the N lattice sites and A is a skew-symmetric matrix. The Pfaffian of matrix A is defined as $\mathrm{Pf}(A) = \frac{1}{2^n n!}\sum_{\tau\in S_{2n}} sgn(\tau)\prod_{m=1}^{n} A_{\tau(2m-1),\tau(2m)}$ with $n = 2N$, where S_{2n} is the set of permutation and $sgn(\tau)$ is the corresponding sign of that. The Z_2 topological invariant is defined as $M = sgn[\mathrm{Pf}(A)]$ when choosing the periodic boundary condition. The Z_2 topological non-trivial phase is characterized by $M = -1$, where as the topological trivial phase corresponds to $M = 1$.

[1] K. Samokhin, Annals of Physics **324**, 2385 (2009).
[2] S. M$\ddot{u}$lbauer, B. Binz, F. Jonietz, C. Pfleiderer, A. Rosch, A. Neubauer, R. Georgii, and P. Bni, Science **323**, 915 (2009).
[3] X. Z. Yu, Y. Onose, N. Kanazawa, J. H. Park, J. H. Han, Y. Matsui, N. Nagaosa, and Y. Tokura, Nature **465**, 901 (2010).
[4] S. Seki, X. Z. Yu, S. Ishiwata, and Y. Tokura, Science **336**, 198 (2012).
[5] K. V. Samokhin, Phys. Rev. B **70**, 104521 (2004).
[6] V. P. Mineev and K. V. Samokhin, Phys. Rev. B **78**, 144503 (2008).
[7] A. P. Schnyder and S. Ryu, Phys. Rev. B **84**, 060504 (2011).
[8] P. M. R. Brydon, A. P. Schnyder, and C. Timm, Phys. Rev. B **84**, 020501 (2011).
[9] S. Fujimoto, Phys. Rev. B **72**, 024515 (2005).
[10] S. K. Yip, Phys. Rev. B **65**, 144508 (2002).
[11] L. Tarruell, D. Greif, T. Uehlinger, G. Jotzu, and T. Esslinger, Nature **483**, 302 (2012).
[12] T. Müller, S. Fölling, A. Widera, and I. Bloch, Phys. Rev. Lett. **99**, 200405 (2007).
[13] G. Wirth, M. Olschlager, and A. Hemmerich, Nat Phys **7**, 147 (2011).
[14] P. Soltan-Panahi, D.-S. Luhmann, J. Struck, P. Windpassinger, and K. Sengstock, Nat Phys **8**, 71 (2012).
[15] C. V. Parker, L.-C. Ha, and C. Chin, Nat Phys **9**, 769 (2013).

[16] T. Kock, M. Ölschläger, A. Ewerbeck, W.-M. Huang, L. Mathey, and A. Hemmerich, Phys. Rev. Lett. **114**, 115301 (2015).

[17] For a perspective and brief review, see, for example, Lewenstein, M. & Liu, W. V. Optical lattices: Orbital dance. *Nat Phys* **7**, 101-103 (2011).

[18] K. Sun, W. V. Liu, A. Hemmerich, and S. Das Sarma, Nat Phys **8**, 67 (2012).

[19] X. Li, E. Zhao, and W. V. Liu, Nat Commun **4**, 1523 (2013).

[20] B. Liu, X. Li, B. Wu, and W. V. Liu, Nat Commun **5**, 5064 (2014).

[21] C. Wu, Phys. Rev. Lett. **100**, 200406 (2008).

[22] C. Wu, Phys. Rev. Lett. **101**, 186807 (2008).

[23] S.-L. Zhang and Q. Zhou, Phys. Rev. A **90**, 051601 (2014).

[24] W. Zheng and H. Zhai, Phys. Rev. A **89**, 061603 (2014).

[25] S. K. Baur, M. H. Schleier-Smith, and N. R. Cooper, Phys. Rev. A **89**, 051605 (2014).

[26] V. Galitski and I. B. Spielman, Nature **494**, 49 (2013).

[27] H. Zhai, International Journal of Modern Physics B **26**, 1230001 (2012).

[28] R. A. Hart, P. M. Duarte, T.-L. Yang, X. Liu, T. Paiva, E. Khatami, R. T. Scalettar, N. Trivedi, D. A. Huse, and R. G. Hulet, Nature **519**, 211 (2015).

[29] Y.-a. Liao, A. S. C. Rittner, T. Paprotta, W. Li, G. B. Partridge, R. G. Hulet, S. K. Baur, and E. J. Mueller, Nature **467**, 567 (2010).

[30] G. B. Partridge, W. Li, R. I. Kamar, Y.-a. Liao, and R. G. Hulet, Science **311**, 503 (2006).

[31] M. W. Zwierlein, A. Schirotzek, C. H. Schunck, and W. Ketterle, Science **311**, 492 (2006).

[32] N. Gemelke, E. Sarajlic, and S. Chu, arXiv **:1007.2677** (2010).

[33] C. Qu, Z. Zheng, M. Gong, Y. Xu, L. Mao, X. Zou, G. Guo, and C. Zhang, Nat Commun **4**, 2710 (2013).

[34] W. Zhang and W. Yi, Nat Commun **4**, 2711 (2013).

[35] Y. Xu and C. Zhang, International Journal of Modern Physics B **29**, 1530001 (2015).

[36] X. Li, Z. Zhang, and W. V. Liu, Phys. Rev. Lett. **108**, 175302 (2012).

[37] E. Zhao and W. V. Liu, Phys. Rev. Lett. **100**, 160403 (2008).

[38] Y.-J. Lin, K. Jimenez-Garcia, and I. B. Spielman, Nature **471**, 83 (2011).

[39] L. W. Cheuk, A. T. Sommer, Z. Hadzibabic, T. Yefsah, W. S. Bakr, and M. W. Zwierlein, Phys. Rev. Lett. **109**, 095302 (2012).

[40] P. Wang, Z.-Q. Yu, Z. Fu, J. Miao, L. Huang, S. Chai, H. Zhai, and J. Zhang, Phys. Rev. Lett. **109**, 095301 (2012).

[41] A. P. Schnyder, S. Ryu, A. Furusaki, and A. W. W. Ludwig, Phys. Rev. B **78**, 195125 (2008).

[42] R. Yamazaki, S. Taie, S. Sugawa, K. Enomoto, and Y. Takahashi, Phys. Rev. A **87**, 010704 (2013).

[43] K. Goyal, I. Reichenbach, and I. Deutsch, Phys. Rev. A **82**, 062704 (2010).

[44] M. J. Bijlsma, B. A. Heringa, and H. T. C. Stoof, Phys. Rev. A **61**, 053601 (2000).

[45] M. A. Baranov, M. Dalmonte, G. Pupillo, and P. Zoller, Chemical Reviews **112**, 5012 (2012).

[46] A. Y. Kitaev, Phys. Usp. **44**, 131 (2001).

[47] P. Ghosh, J. D. Sau, S. Tewari, and S. Das Sarma, Phys. Rev. B **82**, 184525 (2010).

[48] S. Gupta, Z. Hadzibabic, M. W. Zwierlein, C. A. Stan, K. Dieckmann, C. H. Schunck, E. G. M. van Kempen, B. J. Verhaar, and W. Ketterle, Science **300**, 1723 (2003).

[49] C. A. Regal and D. S. Jin, Phys. Rev. Lett. **90**, 230404 (2003).

[50] Y. Shin, C. H. Schunck, A. Schirotzek, and W. Ketterle, Phys. Rev. Lett. **99**, 090403 (2007).

[51] C. Qu, M. Gong, Y. Xu, S. Tewari, and C. Zhang, arXiv **:1310.7557** (2013).